2.9 Å Crystal structure of ligand-free tryptophanyl-tRNA synthetase: Domain movements fragment the adenine nucleotide binding site

VALENTIN A. ILYIN,[1] BRENDA TEMPLE,[1] MEI HU,[1] GENPEI LI,[2] YUHUI YIN,[3] PATRICE VACHETTE,[4] AND CHARLES W. CARTER, JR.[1]

[1]Department of Biochemistry and Biophysics, University of North Carolina, Chapel Hill, North Carolina 27514
[2]Department of Physical Chemistry, Peking University, Beijing, Peoples Republic of China
[3]Department Molecular Biophysics and Biochemistry, Yale University, New Haven, Connecticut 06520
[4]LURE, Orsay, France

Abstract

The crystal structure of ligand-free tryptophanyl-tRNA synthetase (TrpRS) was solved at 2.9 Å using a combination of molecular replacement and maximum-entropy map/phase improvement. The dimeric structure ($R = 23.7$, $R_{\text{free}} = 26.2$) is asymmetric, unlike that of the TrpRS tryptophanyl–5′AMP complex (TAM; Doublié S, Bricogne G, Gilmore CJ, Carter CW Jr, 1995, *Structure 3*:17–31). In agreement with small-angle solution X-ray scattering experiments, un-liganded TrpRS has a conformation in which both monomers open, leaving only the tryptophan-binding regions of their active sites intact. The amino terminal αA-helix, TIGN, and KMSKS signature sequences, and the distal helical domain rotate as a single rigid body away from the dinucleotide-binding fold domain, opening the AMP binding site, seen in the TAM complex, into two halves. Comparison of side-chain packing in ligand-free TrpRS and the TAM complex, using identification of nonpolar nuclei (Ilyin VA, 1994, *Protein Eng 7*:1189–1195), shows that significant repacking occurs between three relatively stable core regions, one of which acts as a bearing between the other two. These domain rearrangements provide a new structural paradigm that is consistent in detail with the "induced-fit" mechanism proposed for TyrRS by Fersht et al. (Fersht AR, Knill-Jones JW, Beduelle H, Winter G, 1988, *Biochemistry 27*:1581–1587). Coupling of ATP binding determinants associated with the two catalytic signature sequences to the helical domain containing the presumptive anticodon-binding site provides a mechanism to coordinate active-site chemistry with relocation of the major tRNA binding determinants.

Keywords: ATP binding site; induced fit; maximum entropy; nonpolar nuclei; tryptophanyl-tRNA synthetase

Tryptophanyl-tRNA synthetase (TrpRS) catalyzes tryptophan activation by ATP and its subsequent aminoacylation to tRNA$^{\text{Trp}}$. TrpRS belongs to the class I aminoacyl-tRNA synthetase family, whose members contain catalytic signatures with consensus sequences, HIGH (Webster et al., 1984) and KMSKS (Hountondji et al., 1986). These "signature" sequences occur at each end of a supersecondary structure called the Rossmann dinucleotide-binding fold, but are brought close to each other in the tertiary structure by a pronounced twist of the four-stranded parallel β-sheet, to form much of the adenine-nucleotide binding site (Carter, 1993).

The previously solved crystal structure of TrpRS complexed with tryptophanyl-5′AMP (TAM) (Doublié et al., 1995) showed that the TrpRS monomer contained two unequal domains. A Ross-mann dinucleotide-binding fold (RF) domain of ~200 residues contained the active sites for adenylation and acyl transfer. A small four-helix bundle of roughly 95 residues contained a putative binding site for the tRNA$^{\text{Trp}}$ anticodon. Comparison with the structure of the closely related tyrosyl-tRNA synthetase (TyrRS) from the same organism (Brick et al., 1988) revealed that the four-helix bundle assumed different orientations in the two proteins, suggesting that the two structures might be "conformational isomers," each capable of assuming an alternate conformation similar to that observed for the other (Doublié et al., 1995).

Domain movements in TrpRS would be relevant to understanding its enzymatic mechanism. Specific recognition by TrpRS of its substrates, tryptophan and tRNA$^{\text{Trp}}$, is crucial to the fidelity of protein synthesis. Equally important are the mechanisms by which the two specific recognition steps embodied in aminoacid activation and acyl transfer are coordinated. Previous work has shown that the anticodon is the dominant identity element for many, if not

all, class I aminoacyl tRNA synthetases (Schulman & Pelka, 1988; Schulman & Pelka, 1989; Jahn et al., 1991; Senger et al., 1992; Yesland & Johnson, 1993). This nearly exclusive dependence on the anticodon for tRNA recognition is surprising in light of the 45–60 Å distance between the anticodon and the 3′ terminal acceptor base. It suggests that coordination of the two specific recognition steps proceeds by intramolecular communication (Rould & Steitz, 1992; Carter, 1993). Such intramolecular communication could be mediated by domain movements.

Conformational changes are also implied by mechanistic studies of activation. Fersht (1987) concluded from detailed enzymatic analysis of TyrRS active-site mutants that the KMSKS and another mobile loop enveloped the transition state in an induced-fit mechanism that implied significant conformational changes in these loops. However, until now there have been no structural data regarding the nature or extent of conformational changes along the proposed reaction pathway for any class I aaRS. Nor has evidence been obtained for how these changes might be coupled to tRNA recognition.

We crystallized and solved the ligand-free TrpRS structure to gain further insight into conformational changes involved in binding Trp and ATP and forming tryptophanyl-5′-adenylate (Trp-5′AMP, TAM). The conformational differences we see are similar to those prefigured in the comparison of TrpRS with TyrRS: the helical bundles of both monomers rotate out, away from the active site, assuming an orientation similar to that seen in the TyrRS structure (Doublié et al., 1995). Moreover, small-angle X-ray scattering shows that these changes also occur in solution and are thus associated with an intrinsic, ligand-dependent molecular polymorphism.

Details of this motion are, however, quite unexpected. We had naively presumed that the domain boundary would be defined by the secondary structures of the Rossmann fold (RF) and helix bundle. In fact, the functional domain boundary lies within the RF domain itself.

Four chain segments from the RF domain bind the adenylate moiety (Fig. 1; Kinemage 1). In the absence of ligands, this configuration unfolds substantially; the N-terminal αA helix rotates 11–15° away from what remains of the RF. Consequently, both signature sequences move by 4–6 Å, together with the helical bundle, creating a more extensive domain that we call the "Small Domain" (SD) and that moves as a rigid body. As a result of this conformational change, ATP-binding determinants within the two signature sequences separate from those in the second crossover connection of the Rossmann fold, fragmenting the ATP binding site in the ligand-free structure into two parts.

Interactions between the N-terminal helix of the RF and the helix bundle are mediated by the highly conserved isoleucines, Ile16 of the TIGN signature and Ile20, which make extensive side-chain packing contacts inside the four-helix bundle. Opening of the active site with rupture of the ATP binding site in this manner may, therefore, reflect general induced-fit mechanisms for substrate binding and for product release during acyl transfer in all class I tRNA synthetases.

Results

Small-angle scattering

How X-ray crystal structures relate to structures in solution is always an implicit question, but it is seldom addressed explicitly.
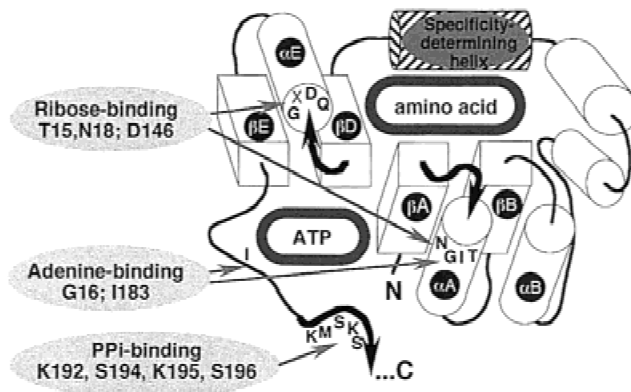

Fig. 1. Schematic diagram of the Rossmann dinucleotide-binding fold domain in TrpRS, showing binding determinants from four different chain segments that surround the adenine nucleotide in the TAM complex structure (Doublié et al., 1995). Two of these segments are the signature sequences, TIGN and KMSKS, that are characteristic of all class I aminoacyl-tRNA synthetases. The others include a highly conserved, GxDQ sequence at the N-terminus of the C-terminal αE helix of the Rossmann fold and an extended chain preceding the KMSKS signature. Secondary structure elements are identified consistently with the scheme proposed by Burbaum for class I aminoacyl-tRNA synthetases (Burbaum et al., 1990). The "specificity-determining helix," αD, contains many of the residues that interact with substrate tryptophan. See Kinemage 1 for a three-dimensional representation.

In the case of TrpRS, however, the possibility that crystal lattice packing may distort the enzyme is important, because we will interpret conformational differences between the unliganded molecule and the TAM complex (Doublié et al., 1995) in terms related to the structural reaction profile. Previous quantitative study of crystal growth (Carter et al., 1994) strongly suggested that TrpRS conformations in solution depended on the pH and on synergistic effects of pH, tryptophan, and ATP concentrations. These effects implied, in turn, that the structures of different TrpRS crystal forms would provide relevant data linking conformational changes and catalysis.

To solidify that link, we (C.W.C and P.V.) therefore performed a detailed factorial study of the radius of gyration by small angle X-ray scattering (SAXS) in undersaturated solutions, similar to those used to grow crystals. The TrpRS radius of gyration measured in these solution experiments depends on both the ligation state [being most compact in the presence of high (ATP)] and on the pH (being most compact at high pH). Details of this study will be published separately, but solution measurements corresponding most closely to the ligand-free crystal structure described here and that published for the TAM complex are summarized in Table 1.

Agreement is excellent between the radii of gyration estimated from solution X-ray scattering and those calculated from the two crystal structures, implying that neither crystal structure shows major distortions induced by lattice-packing contacts. This conclusion extends those drawn from earlier analyses of crystal growth experiments that the open and closed conformations form in response to appropriate ligands, and that crystallization traps predominant conformers from solution. It also underscores the importance of using cocrystallization in preference to soaking ligands into pregrown crystals.

Table 1. *Radii of gyration observed in solution and in the crystalline state*

Sample	$\langle Rg_{SAXS} \rangle$[a] (No. replicates)	Rg_{XTAL}[b]
Ligand-free TrpRS, pH = 6.8	32.5 ± 0.33 Å; (10)	32.02 ± 0.07 (3) Å
TrpRS:trp-5′AMP complex, pH = 7.5	30.2 ± 0.29 Å; (3)	29.95 (1) Å

[a] Radii of gyration in solution were calculated from the slopes of Guinier plots after background scattering had been subtracted. Channels at very low resolution, showing evidence of small amounts of aggregation, were eliminated from the calculation. Standard deviations of the mean values were calculated on the basis of the numbers of observations given in parentheses.
[b] Atomic coordinate files were used to generate estimates of the radii of gyration from solution, using an estimate for the effects of bound water, without optimization of the bound-water contribution.

Ligand-free TrpRS monomer conformation and comparison with that of the TAM complex

Ligand-free *Bacillus stearothermophilus* TrpRS is highly polymorphic and crystallizes either in triclinic (P1) or monoclinic (C2) forms (Table 2). Comparison of the ligand-free structures with that of the TAM complex (Doublié et al., 1995) shows a significant rotation of the helical domain outward by about 13° from the dimer interface in the ligand-free structure (Fig. 2B,C). This movement increases the overall length of the ligand-free dimer, consistent with the increased radius of gyration observed by solution X-ray scattering (Table 1).

From the electron density map produced by rigid-body refinement and model-independent phase improvement, it became clear that much of the N-terminal helix in the Rossmann fold, αA (Thr15–Gln30), had moved as a rigid body together with the helical domain (Ile183–Met293). These two segments form what we will call the "small domain," SD, and we will designate the remaining fragment of the Rossmann fold domain, together with the C-terminal helix 294–321, as RF-αA.

Table 2. *Crystallographic data*

Unit cell	P1	C2
	Triclinic	Monoclinic
	$a = 91.66$,	$a = 226.72$,
	$b = 122.51$,	$b = 91.66$,
	$c = 124.91$,	$c = 156.97$,
	$\alpha = 78.67$,	$\beta = 132.66$
	$\beta = 68.86$,	
	$\gamma = 68.65$	
Resolution	3.5 Å	2.9 Å
$\langle I \rangle / \langle \sigma \rangle$	6.95	7.95
R_{merge}	0.115	0.091
Number of reflections	29,595	39,287
Redundancy	1.8	1.8
Completeness (last shell)	68% (52%)	75% (55%)
Refinement		
R_{factor}[a]		0.25
F_{free}[b]		0.28
RMSD (bonds, Å)		0.009
RMSD (angles, deg)		1.14
Acceptable (ϕ, ψ) angles (%)		90.2

[a] $R = \sum(|F_{obs}| - |F_{calc}|)^2 / \sum(|F_{obs}|)^2$.
[b] Based on 5% of the total number of reflections.

Notably, the SD defined by the domain motion contains both signature sequences, TIGN and KMSKS, which interact with the ribose and pyrophosphate moieties in the transition state for tyrosine activation by TyrRS (Fersht, 1987; Fersht et al., 1988), and so are of central importance to catalysis of amino acid activation. Previously, they were considered to belong to the RF domain. Their displacement away from the RF-αA domain, and hence, from the active site in ligand-free TrpRS is the most unexpected and significant conclusion of this study.

We will discuss, in turn, the six monomer conformations within the asymmetric unit of ligand-free TrpRS crystals, relationships between these structures and that of the TAM complex, functionally significant consequences of the domain movement at the active site and elsewhere, and patterns of side-chain packing that underlie it.

Noncrystallographic symmetry and domains: Analysis of rigid bodies (animated in Kinemage 2)

Multiple subunits in an asymmetric unit pose the question of how well structures of related molecules resemble one another. Root-mean-square deviations (RMSDs) between subunits cannot distinguish between randomly distributed structural deviations and deviations resulting from rigid-body domain movement. An appropriate way to answer this question is through the identification of rigid bodies within the monomers (Baldwin & Chothia, 1979), together with the imposition of their noncrystallographic structural equivalence during refinement. The six monomers per asymmetric unit provide an ample database for such an analysis. Thus, definition and analysis of rigid bodies in ligand-free TrpRS were intimately related to the structure refinement.

Attempts to impose noncrystallographic equivalence between the six monomers during refinement gave high RMSDs between subunits and also high values for the R_{factor} and R_{free} (Fig. 3A). Pairing monomers into dimers and applying only threefold noncrystallographic symmetry improved both statistics. Dividing each monomer into two domains (RF-αA and SD) and applying noncrystallographic symmetry constraints between equivalent domains further decreased the RMSDs by nearly an order of magnitude, without compromising the refinement statistics (Fig. 3B), showing with high statistical significance that ligand-free TrpRS is both asymmetric and polymorphic. SD conformations for the six monomers superimposed on a subset of Ca atoms in the RF-αA domain (Doublié et al., 1995) are animated in Kinemage 2.

Structural differences between the six monomers result almost exclusively from variations in the outward motion of the SD, relative to its configuration in the TAM complex. The monomer-to-
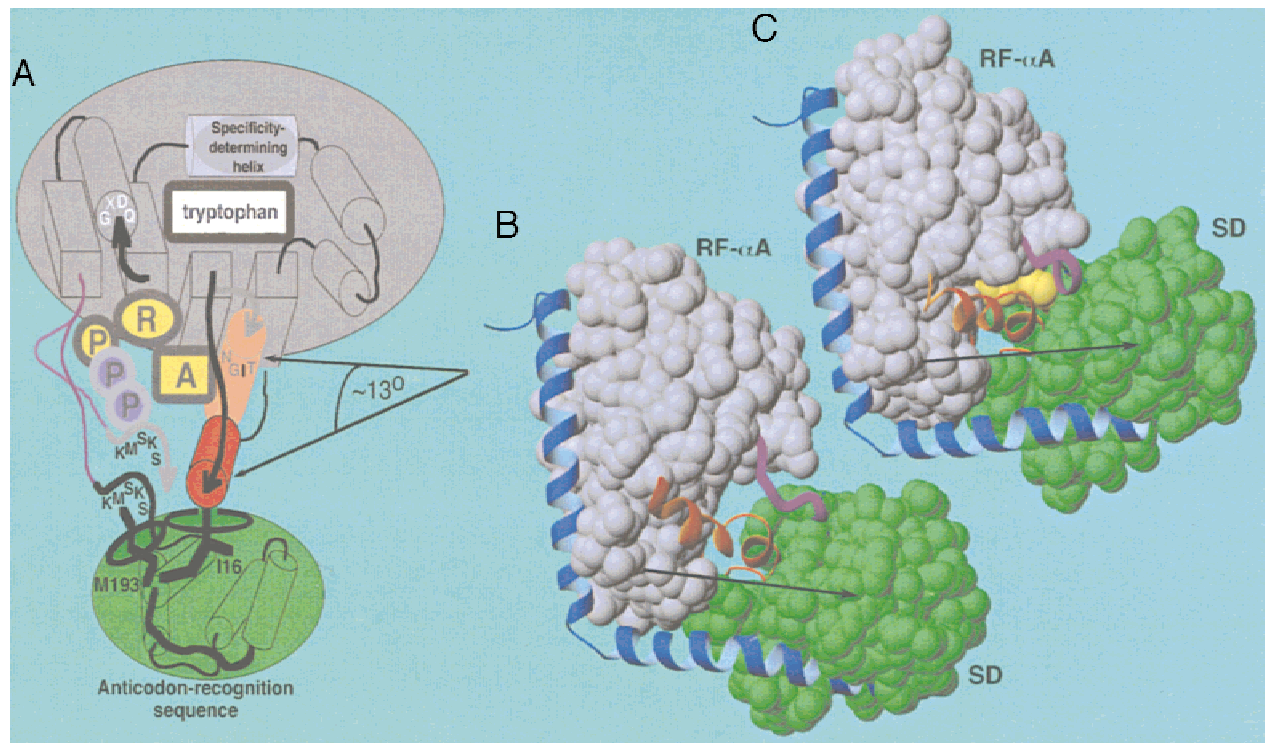
Fig. 2. Domain movement and active site fragmentation. Colors used in **A–C:** small domain (SD; green), Rossmann fold (RF-aA; gray), AMP (yellow), αA helix (orange), long belt (purple), and the C-terminal helices (blue). **A:** Schematic drawing of the TrpRS monomer, viewed directly into the active site. The axis of domain motion is roughly horizontal and in the plane of the figure. The two signature sequences are anchored to the SD via nonpolar interactions involving I16 (TIGN) and M193 (KMSKS). **B,C:** Structures of ligand-free and the TAM complex monomers, viewed roughly 90° around the vertical axis from the orientation in **A** to emphasize the domain motion. Rigid parts of the structure are indicated in **B** and **C** by space-filling atoms; flexible parts by ribbons. Arrows connect the center of domain rotation to the SD center of mass.

monomer variation of the angle $\Delta\alpha$ subtended by the centers of mass in the two domains in ligand-free TrpRS and the TAM complex on the axis around which they rotate (Table 3), illustrates the interdomain flexibility. The average $\Delta\alpha$ value of 13° between the ligand-free and TAM complex conformations is about seven times the standard deviation of the different $\Delta\alpha$ values, suggesting that TrpRS has at least two conformations and that ligand binding induces the transition between them.
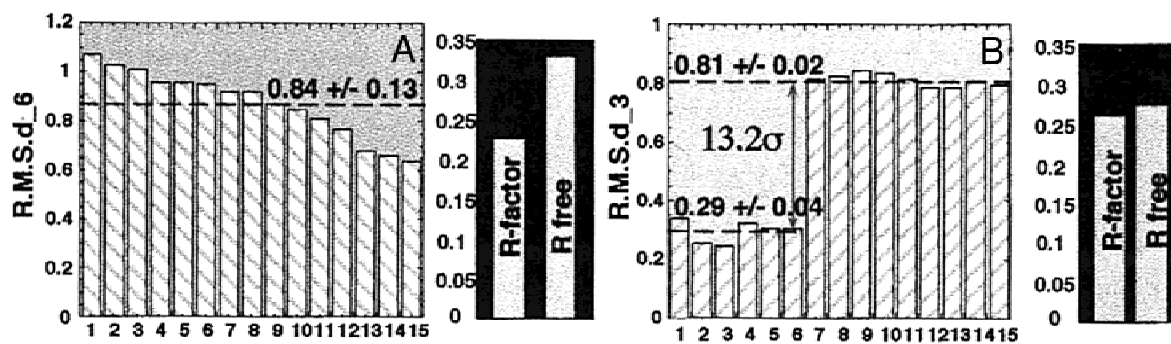

Fig. 3. Intersubunit deviations between six ligand-free TrpRS monomers. **A:** Under sixfold averaging, there is no apparent clustering of RMSDs, and the mean value and standard deviation are both large. **B:** Under threefold averaging, the nine RMSDs between "unlike" monomers are larger than the six between "like" monomers by ~13 times the standard deviation of the respective mean values. *R*-factors for working and test data are shown in the second histogram for each comparison. Allowing molecular asymmetry led to a substantial reduction in the R_{free} value.

Table 3. *Noncrystallographic variation of Δα from monomer to monomer*

Monomer	A	D	B	E	C	F
Δα-angle (deg)	14.8	12.2	14.6	10.5	11.4	11.5

Ligand-free and TAM complex conformations differ by localized changes in backbone dihedrals (φ,ψ) in two "belts" connecting the domains (animated in Kinemages 3, 4, and 5)

Structural differences between monomers in ligand-free TrpRS and in the TAM complex are highlighted by plotting absolute differences in the Ramachandran angles, φ and ψ (Fig. 4). Changes
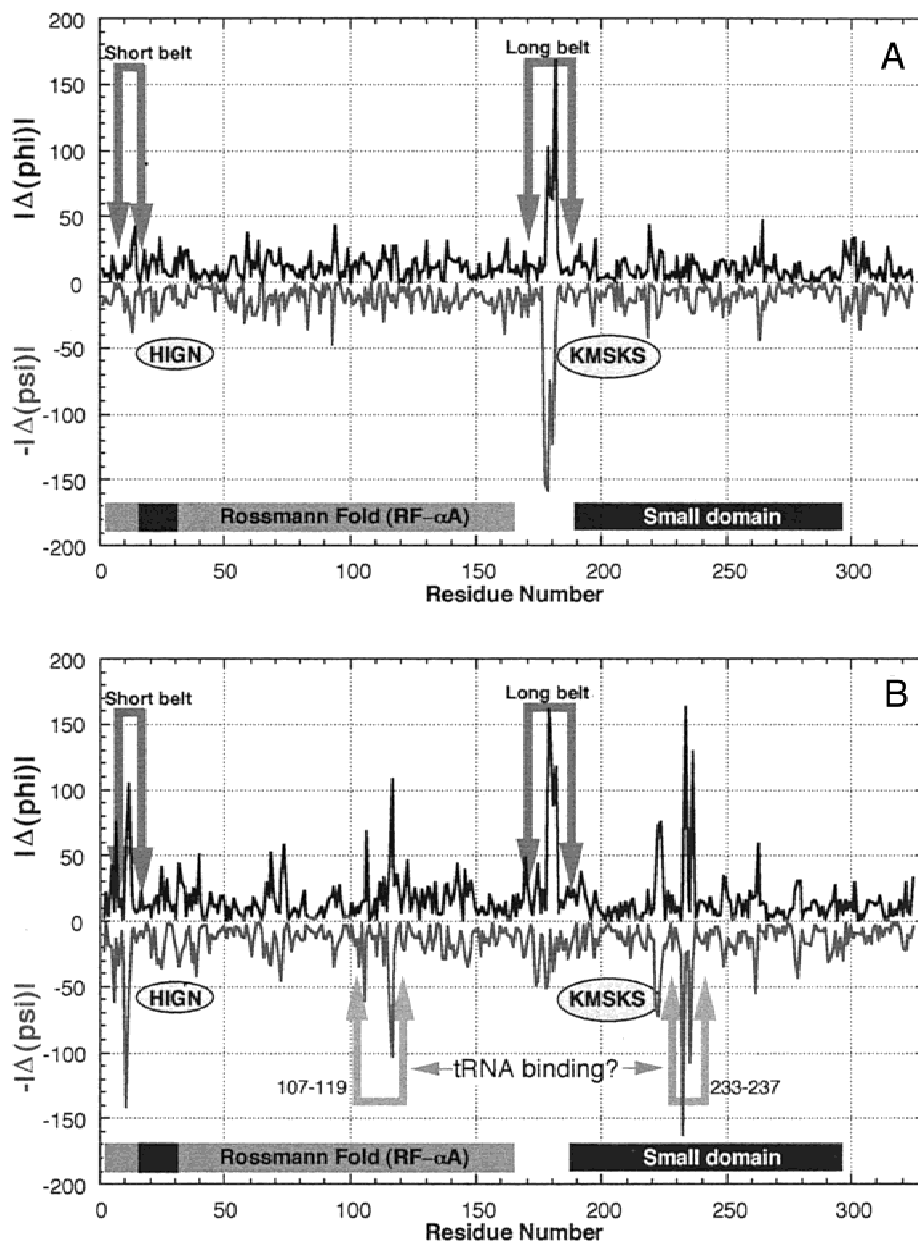

Fig. 4. Localization of conformation changes visualized by Ramachandran angle difference plots. **A:** Differences between monomers A and D of one of the dimers in the asymmetric unit. The absolute values of differences between corresponding (φ,ψ) angles are plotted vs. residue number. The short and long belts are defined in the text. Locations of the two signatures characteristic of class I aaRS are indicated, as are the extents of the Rossmann fold and small domain. The dark gray box near residues 16–29 constitutes the N-terminal αA helix of the Rossmann fold. **B:** Differences between the A monomer in the ligand-free asymmetric unit and the monomer in the TAM complex.

within the ligand-free asymmetric unit, as animated in Kinemage 2, are limited to short segments before and after the αA helix, and a longer segment at the end of the final β-strand in the RF-αA (Fig. 4A; Kinemage 3), confirming that rigid body motion accounts for the different conformers.

The loop Arg175–Ile183 following the final β-sheet of RF-αA immediately precedes the KMSKS signature and connects the two domains. This segment is the most conspicuous feature of all differential {φ,ψ} plots (Fig. 4A). We will refer to it as the "long belt." In the ligand-free structure, the long belt is extended; it closes markedly in the TAM complex.

A second, discrete change involves Pro10–Gly12, preceding the αA helix and beginning with the highly conserved Pro10, described as the proline "wedge" (Burbaum & Schimmel, 1992). As it lies opposite the active site from the long belt, allowing movement of the N-terminus of the αA helix away from the RF-αA and together with SD, we call this segment the "short belt." In ligand-free TrpRS, this short belt is fully extended, limiting further opening of the small domain. Movement of the amino terminus of the αA helix also involves an unusual five-residue turn around Gly21 and flexibility of a loop 29–33 connecting the αA helix and βA strand.
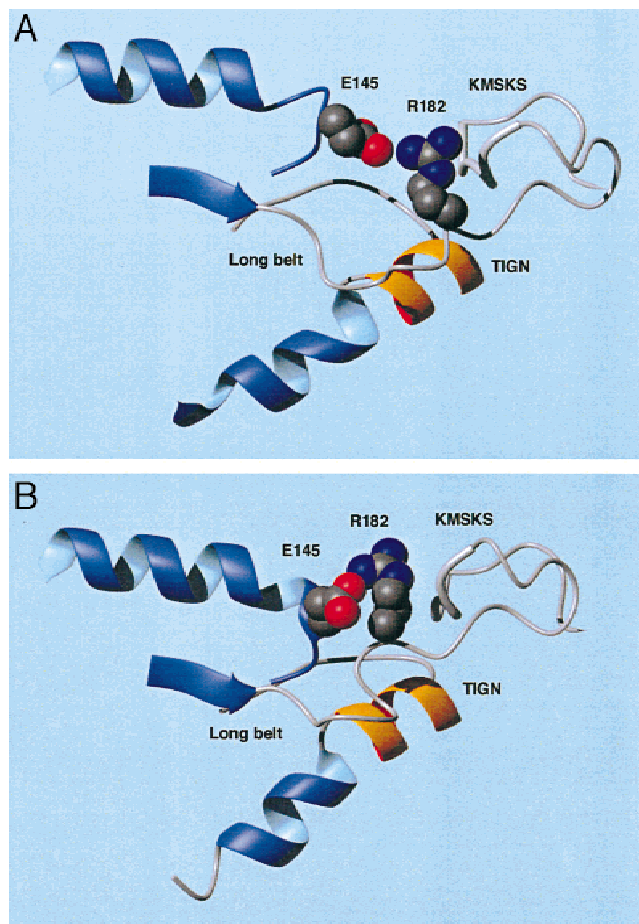
Finally, the two domains are also linked by two long, C-terminal α-helixes. The first, residues 265–293, belongs to the SD; the second, residues 295–321, to RF-αA. No significant changes are localized to any residues connecting these two helixes (Figs. 2, 4). Instead, as animated in Kinemages 4 and 5, there are cooperative bending motions over their entire lengths.

An electrostatic switch (animated in Kinemage 6)

Liganded and ligand-free TrpRS conformations are characterized by alternate configurations of an ionic, hydrogen-bonded interaction between Glu145 and Arg182. In the TAM complex (Fig. 5B), these two residues are close to each other and make significant hydrophobic contacts; in the extended ligand-free conformation (Fig. 5A), the residues move apart, retaining the hydrogen-bonded connection between them. Both hydrogen bonds are reinforced by electrostatic attractions between oppositely charged groups. They are, therefore, of significant strength and constitute distinct energy minima, separated by the barrier imposed by reconfiguring the hydrogen bond. (This reconfiguration could conceivably occur either by breaking the hydrogen bond and re-forming it, or by maintaining it while rotating the side-chain dihedral angles of Glu145 and Arg182 through unfavorable intermediate positions. Either possibility imposes an energy barrier to the change.) Thus, they comprise an electrostatic "switch," restricting TrpRS conformations to those close to the open and closed states.

Domain movement has significant impact on active-site architecture, especially in the ATP binding site (animated in Kinemage 6)

Independent superposition of the SD and RF-αA in both structures shows that the two domains are affected differently by ligand binding. The SD remains quite rigid (Fig. 6); the RMSD between the ligand-free and TAM structures is 0.49 Å. In contrast, that between corresponding parts of the RF-αA in the two molecules is 0.73 Å.

The main portion of the RF-αA domain constitutes the tryptophan binding site and the dimer interface. The tryptophan binding site is bounded on four sides by the N-terminal βA strand of the
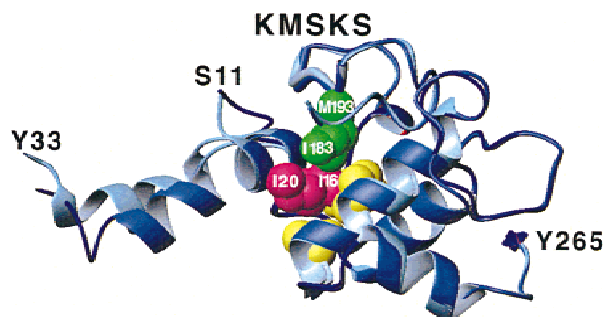

Fig. 5. "Electrostatic switch" involving alternate configurations of Glu145 and Arg182. In the open conformation **A**, both amino acids extend toward each other; while in the closed conformation **B**, their Cα atoms are close enough that their side chains engage in extensive Van der Waals contacts.

Fig. 6. Superposition of the small domain from two structures. SD moves as a rigid body, RMS of main-chain atoms between ligand-free and TAM small domains is 0.54 Å. The αA-helix (15–30) from RF moves together with SD and may work as a spring. Space-filling representations of residues Ile16, Ile20 (magenta), I183, Met193 (green), Ile204, Ile244, and Leu248 (yellow) that provide nonpolar interactions joining the three distant fragments of the SD together, are color coded.

Rossmann fold, residues 1–9; the specificity determining helix, αD, residues 120–136; the mobile loop/helix, residues 106–117; and the C-terminal helix of the Rossmann fold, αE, residues 142–165. These four elements open somewhat in ligand-free TrpRS, leaving the tryptophan binding site slightly larger than it is in the TAM complex. Thus, the RF-αA fragment is surprisingly fluid, a point to which we will return in a subsequent discussion of side-chain repacking.

Important differences between ligand-free TrpRS and the TAM complex active sites are illustrated in Figure 7 and animated in Kinemage 6. Movement of the SD effectively removes the αA helix, together with both signature sequences TIGN and KMSKS and the long belt 175–182, from their proximity to the active site in the TAM complex. Thus, of the binding determinants illustrated schematically in Figure 1, only the fourth determinant, residues

144–145, remains with the RF-αA domain, and the adenine nucleotide binding site is fragmented in ligand-free TrpRS by an ~4 Å separation of its two complementary parts.

Binding of ATP to the SD region of ligand-free TrpRS containing the signature sequences could utilize three of the four binding determinants while keeping the bound ATP from interfering with subsequent binding of tryptophan. The open configuration in ligand-free TrpRS thus affords equal, independent access to either tryptophan or ATP, and either substrate could, in principal, bind first to the ligand-free conformation. This situation contrasts with that in the TAM complex, in which the adenine moiety reduces the static accessibility to the tryptophan binding site from 27 to 3 Å^2. A similar observation was made for the tyrosyl-tRNA synthetase:tyr-5''AMP complex, and it was argued (Brick et al., 1988) on that basis that an ordered binding mechanism was more likely.
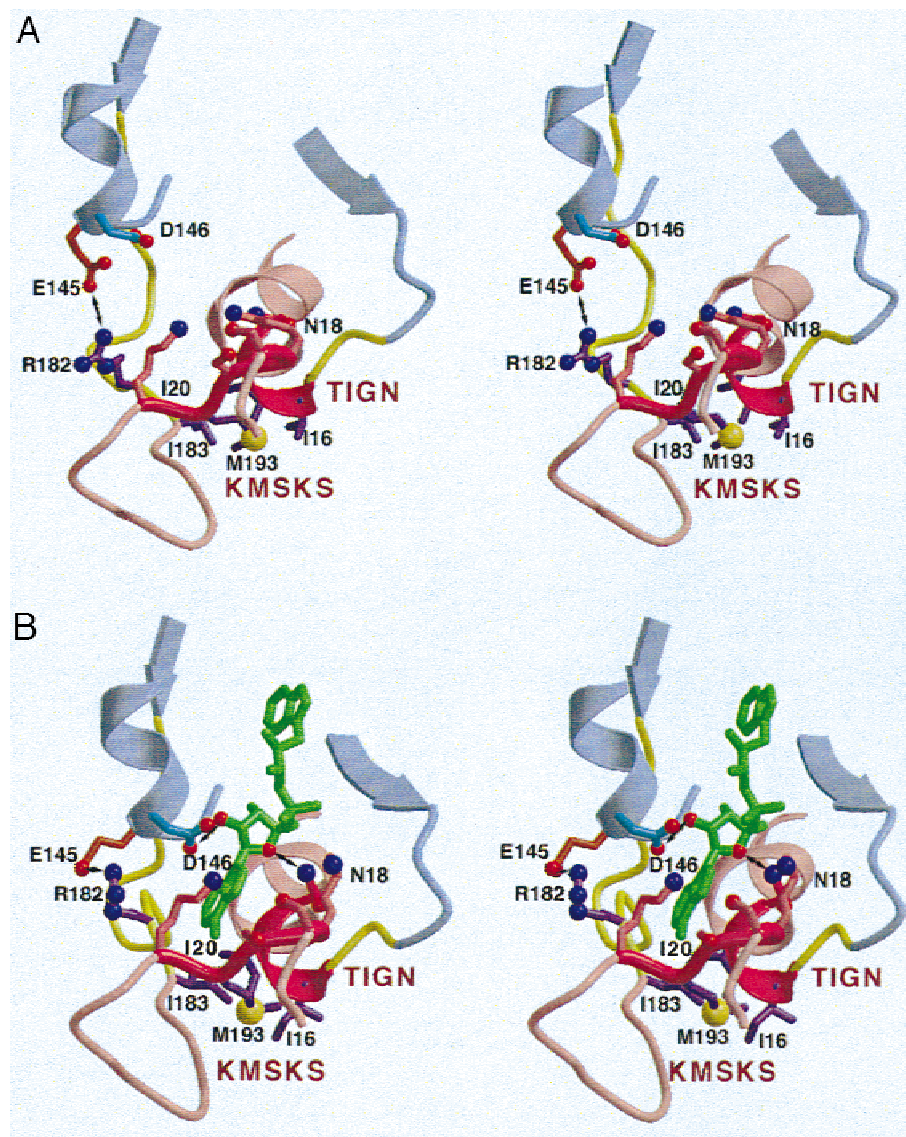

Fig. 7. A: Fragmentation of the ATP binding site in ligand-free TrpRS. **B:** Corresponding view of the TAM complex. In both **A** and **B**, Rossmann-fold segments are blue, small domain segments are red, the two belts are yellow, and trp-5′AMP (TAM) is green. Signature sequences are highlighted by bright red. Interactions to ribose from both RF-αA and SD are shown by arrows.

The most obvious of the new interactions in the complexed form that arise across the interdomain interface are two hydrogen bonds formed between TrpRS and the tryptophanyl-5′adenylate. These link the 2′ ribose hydroxyl group to the carboxylate of Asp146 and the 4′ glycosidic oxygen to the amide nitrogen of Asn18 in the TIGN signature. The two conformations are distinguished, therefore, by opening and closure of binding determinants onto the ribose of the adenine nucleotide.

Domain movement is coupled to localized changes in two regions implicated in binding of cognate tRNA^Trp

Two other short peptides change conformational angles abruptly between the liganded and ligand-free conformations (Fig. 4B). The first, residues 117–119, lies within the Rossmann fold, bordering the tryptophan binding site. This segment represents the vestige (or ancestor) of what in the glutaminyl-tRNA synthetase is called the acceptor binding domain (Rould et al., 1989). The second, residues 233–237, lies within the SD, opposite the extended chain containing residues homologous to the segment in GlnRS that interacts with the U35 of the glutamine anticodon. Thus, these two regions were both implicated by circumstantial evidence in the binding of the tRNA^Trp substrate (Doublié et al., 1995).

Side-chain repacking (animated in Kinemage 7)

Analysis of internal packing including identification of nonpolar nuclei (NPN-analysis) has been carried out for ligand-free TrpRS and the TAM complex by the method of Ilyin (1994), which identifies contacts between nonpolar parts of all side chains, with a cutoff distance of 4.5 Å and at least two nonpolar atom–atom interactions. Consistent with the rigid-body behavior of supersecondary structure elements, NPN-analysis reveals three distinct core regions in both TrpRS structures, two within the RF-αA plus the SD. Important aspects of side-chain packing associated with each core region are illustrated in Figure 8, which was based on comparing invariant side-chain interactions, common to both structures, and those that change substantially. That comparison can be examined interactively using Kinemage 7.

Nonpolar side-chain packing couples the two signature sequences to the small domain

The TIGN and KMSKS sequences move together between open and closed states. Nonpolar residues from each signature are embedded in an extensive nonpolar interface involving hydrophobic residues Ile183, Ile204, Ile244, and L248 within the SD. The TIGN sequence is held to this nonpolar nucleus by Isoleucines I16 and I20, the KMSKS sequence by Met193 (Fig. 6). The importance of these interactions, which are evidently responsible for the coupled movements of the αA helix and the four-helix bundle, is suggested by the fact that all three residues are conserved throughout the family of class I aminoacyl-tRNA synthetases.

Phe26 and Tyr65 serve as a "bearing" for the domain movement

Significant side-chain repacking occurs within nonpolar clusters between TAM-complexed and ligand-free TrpRS. Changes that accompany reorientation of the αA helix occur within the first
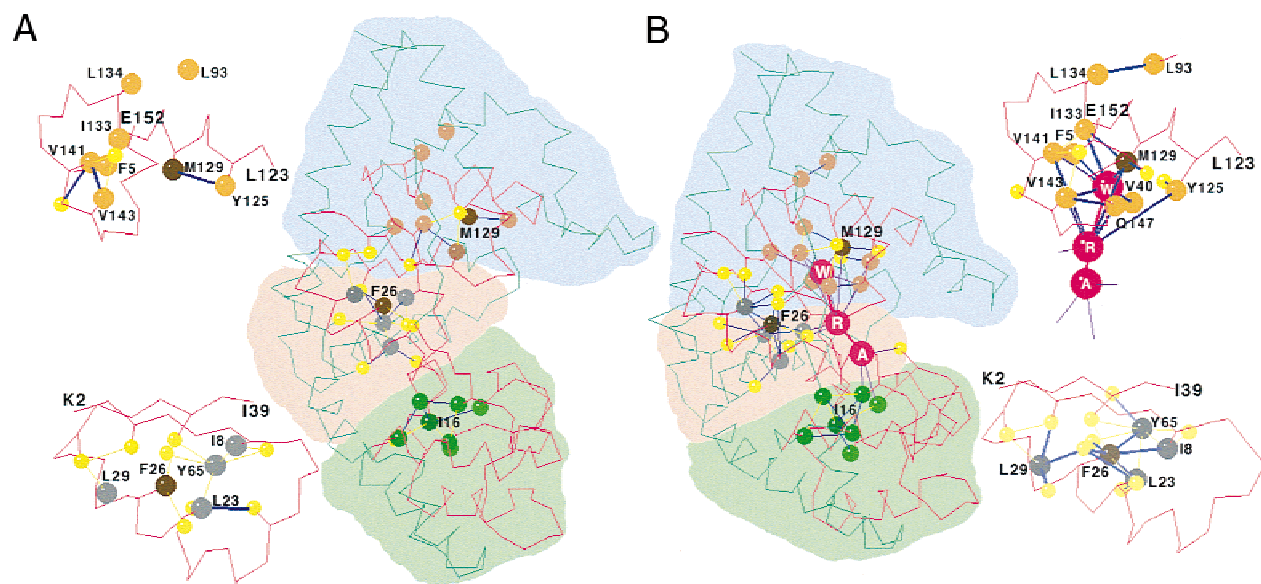

Fig. 8. Nonpolar repacking in (**A**) ligand-free TrpRS and (**B**) TAM complex monomers. Each circle is a side-chain centroid involved in nonpolar contacts, as identified by the method of Ilyin (1994). The monomer drawings are segmented into three core regions, corresponding to the first (rose) and second (blue) halves of the Rossmann fold, and the SD (green). The Cα carbon chain is colored red in regions discussed in the text, and green elsewhere. Large red spheres in **B** represent the centroids of tryptophan (W), ribose (R), and adenine (A) in the bound tryptophanyl-5′AMP. Locations of key residues discussed in the text are indicated by darker coloring and by residue names for I16, F26, and M105. Exploded views show the packing rearrangements involved in tryptophan binding (top; residues 123–152) and in the "bearing" (bottom; residues 2–39). Yellow lines represent inter side chain contacts common to both structures, thicker blue lines represent interactions present in only one of the two structures. Smaller yellow circles represent centroids of neighboring side chains involved in invariant NPN in the two structures.

crossover connection of the Rossmann fold, residues 2–39, and involve Phe26, at the C-terminus of the αA helix, and its close neighbors. In particular, on opening, Phe26 breaks from nonpolar contacts formed with Tyr65, Ile8, Leu23, and Ile70 in the TAM complex. Tyr65 loses contact with Phe26 and joins with Leu77. This exchange of partners suggests that Phe26 and Tyr65 serve as the center of a bearing for the domain movement.

Intensification of packing around the tryptophan binding pocket in the complexed state

Nonpolar packing changes within the second crossover connection of the Rossmann fold generally involve loss of many nonpolar bonds to substrate tryptophan. Met105 and Tyr125 lose contact with the ligand to make contacts with each other, as do Val141 and Val143. A conspicuous rearrangement breaks nonpolar contacts between Gln147 and both substrate and Val143. Contacts across the tryptophan binding site, between Met105 and Ile133, and between Leu93 and Leu134 are broken in ligand-free TrpRS.

Dimer asymmetry and the dimer interface conformation (animated in Kinemage 8)

Data from Figure 3 and Table 3 document the important conclusion that the unliganded TrpRS dimer is asymmetric. The SD assumes a different conformation in each monomer. The three dimers are all asymmetric, generally comprising one monomer with a large angle, $\Delta\alpha \sim 14°$ and one with a small angle, $\Delta\alpha \sim 11°$. In contrast, the interface between the two monomers appears to be surprisingly symmetric. Chain segments contributing to the interface, residues 46–121 and their counterparts from the opposite monomer, a total of 150 residues, can be superimposed on the symmetric TAM complex dimer with an RMSD of 0.54 Å for a subset of 50 corresponding alpha carbon atoms from each monomer (Doublié et al., 1995). Thus, there appears to be little change in the configuration of the dimer interface between the ligand-free and TAM-complexed TrpRS. Nor have we found evidence in the dimer interface for the broken symmetry in the relative rotations of the two small domains. As noted in the discussion, these observations are somewhat inconsistent with other experiments, and should be interpreted with caution.

Discussion

Crystal and solution structure analyses are mutually consistent

Radii of gyration for the ligand-free TrpRS structure reported here and the product complex structure reported previously (Doublié et al., 1995) are closely matched by corresponding values obtained from small angle X-ray scattering from solutions close to those used for crystal growth (Table 1). The consistency of these observations gives us a better understanding not only of the enzymatic processes of binding and catalysis by TrpRS, but also helps rationalize the extensive TrpRS crystal polymorphism. The ligand-free molecule is longer because of the active site opening. The flexible positions of domains in the molecule, which result in different molecular dimensions, may help explain crystallization difficulties with this and similar proteins. The large conformational change would doubtless distort ligand-free crystals upon ligand binding,

making it difficult to effect an undistorted transition of unliganded enzyme to the Trp-5′AMP complex in the same crystal lattice. The magnitude of the observed change thus vindicates our strategy of cocrystallization, as opposed to soaking ligands into previously grown crystals (Carter et al., 1994).

The impact of possible of additional states on functional interpretations

The ligand-free and TAM complex structures we have described for TrpRS likely represent structural states along the TrpRS structural reaction profile during catalysis. Conformational differences between these two structures, however, may not actually represent catalytically relevant, sequential transitions. The previously described TAM complex structure (Doublié et al., 1995) represents a product state, the result of tryptophan activation. A third state, between the free enzyme and adenylate complex, was proposed by Fersht et al. (1988) for TyrRS on the basis of mutagenesis experiments implicating movement of the KMSKS loop in the transition state for activation. Structures recently solved for TrpRS ternary complexes with nonreactive tryptophan analogs plus ATP have a distinct conformation that may represent this third state (Carter et al., 1999) and will be described separately. Additional structural states may occur during tRNA^{Trp} binding, acyl transfer, and product release to regenerate free enzyme from the TAM complex. These considerations suggest that the ligand-free TrpRS structure should be interpreted with caution. Nonetheless, this new structure does complement mechanistic studies of aminoacid activation by other class I aminoacyl-tRNA synthetases.

The induced-fit mechanism of dimeric class I aminoacyl-tRNA synthetases

The domain movements observed in the ligand-free TrpRS structure are in surprisingly detailed accord with the directed mutagenesis and pre-steady state kinetic analysis of the TyrRS mechanism (Fersht, 1987; Fersht et al., 1988). Those studies concluded that residues interacting with the substrate tyrosine had similar binding properties throughout the catalytic cycle, whereas those interacting with the ribose and pyrophosphate moieties of substrate ATP had minor effects on ground-state interactions, achieving maximal binding affinity only in the transition state and the tyrosyl-adenylate product complex. Consistent with that result, the tryptophan binding site in ligand-free TrpRS is essentially intact, and does not change significantly in the TAM complex, whereas the three ATP-binding determinants in the SD move 4 Å away from the fourth determinant at the amino terminus of the αE helix (Fig. 7). The ATP binding site, which is fragmented in ligand-free TrpRS, cannot achieve its full measure of affinity for ATP until the enzyme closes, en route to the transition state. Indeed, the "induced-fit" by which binding determinants for these moieties participate in catalysis involves a profound reorganization of the Rossmann nucleotide binding fold itself, which has tacitly been assumed to be structurally rigid whenever it occurs in a protein.

The previous studies of the TyrRS mechanism suggest that additional aspects of the ligand-free TrpRS structure are relevant to questions regarding substrate binding and amino acid activation. Kinetically, tyrosine activation is a random-order reaction (Fersht, 1987). However, the TyrRS crystal structures are incompatible with a random binding order, because the adenosine moiety blocks

access to the tyrosine binding site. Fersht rationalized the inconsistency by proposing a virtual equilibrium mechanism, noting that the E·ATP complex was in virtual equilibrium with the ternary E·Tyr·ATP complex via the free enzyme, because the off-rate for ATP is an order of magnitude faster than that for tyrosine. The ligand-free TrpRS structure suggests that binding sites for both tryptophan and ATP are open to solvent and accessible to bind either substrate. In other words, ligand-free TrpRS is in good agreement with the TyrRS kinetic analysis. The accessibility of the "open" TrpRS configuration to both substrates is consistent with a random-order reaction for TrpRS, as noted above. If ligand-free TyrRS has a comparable open conformation, as suggested by Doublié et al. (1995), then random-order TyrRS kinetics also would follow naturally from its independent accessibility to both substrates.

Fragmentation of the ATP binding determinants in the open TrpRS conformation is also consistent with the relatively weak ground-state affinity of TrpRS for ATP ($K_m \sim 50~\mu M$) relative to tryptophan ($K_m = 2~\mu M$; M. Hu, unpubl. obs.) and with development of high-affinity binding only in the transition state of the TyrRS mechanism. Particularly interesting is the location of Asp146 in RF-αA. The homologous residue in TyrRS, Asp194, has no role in ground-state ATP binding, but an important role in transition state binding (Fersht, 1987), consistent with our suggestion (above) that the initial ATP binding site may reside in the SD of the open conformation.

A further implication is that when ATP binds, side chains from the two signature sequences in the SD and those from residues 144–147 in RF-αA move closer to the ATP. Active-site closure occurs via the refolding of the short (11–12) and long belts (175–182), the reorientation of the αA helix, and the resetting of the electrostatic switch, E145–R182. Conversely, binding interactions with ATP and especially to the ribose in the closed state provide free energy to help stabilize the closed configuration of the SD, and, as for TyrRS, they may be a key to high transition-state affinity.

The consistency of structural, mutational, and kinetic analysis implies that the adenine nucleotide ribose and pyrophosphate moieties have profound impact on the structural and catalytic behavior of these class I aminoacyl-tRNA synthetases. The ligand-free conformation reveals that the TrpRS conformational polymorphism is intimately coupled to the binding and utilization of ATP. The conformation change is focused explicitly on the reconfiguration of the four ATP binding determinants, which cannot all interact with ATP in the ground state, but which are all assembled appropriately in the closed, product complex. This key observation implies that TrpRS and perhaps, by implication also TyrRS, use the conformation change to modulate binding-site stereochemistry and adenine nucleotide affinity coordinately, for optimal interaction and minimal interference with the aminoacid binding site. It, therefore, provides a significant new structural dimension to the concept of "induced-fit" proposed by Fersht (1988).

Side-chain packing, helix distortion, and the conformational polymorphism

Analysis of side-chain packing between the ligand-free and TAM structures has been carried out by identifying and comparing "nonpolar nuclei" as defined by Ilyin (1994). Noteworthy are signature sequence residues Ile16 and Met193, plus Ile20, whose nonpolar packing interactions within the helical domain are responsible for the rigid-body movement of the two signatures with the SD. It is curious that nonpolar nuclei in the two crossover connections of

the Rossmann fold both repack in the ligand-free state. The most obvious alternative side-chain repacking occurs between the two rigid domains (RF-αA and SD) and side chains, particularly around Phe26, at the C-terminus of the α helix. These internal rearrangements appear to improve side-chain packing, and hence, stabilize the protein conformation of the TAM complex. In contrast, the uniform flexing of the C-terminal α-helices (residues 265–291 and 295–324; Kinemages 4 and 5) suggests that they work as springs. They seem to be destabilizing in the TAM complex and may develop and/or dissipate flexional stress as the SD moves relative to RF-αA. Such balancing of packing and conformational effects, together with the ligand binding free energies, could promote the ligand-dependent conformational polymorphism that underlies the induced-fit mechanism.

Molecular asymmetry and intramolecular communication

Interestingly, comparison of independent sixfold vs. threefold (monomers vs. dimers) averaging shows that ligand-free TrpRS is asymmetric. The closely related TyrRS is also asymmetric in solution (Ward & Fersht, 1988a, 1988b), becoming symmetric only when crystallized, as does the liganded TrpRS structure observed in the tetragonal crystal form (Doublié et al., 1995). TrpRS and TyrRS may have an equivalently asymmetric nature in solution. In light of this asymmetry, our observations on the structural invariance of the dimer interface should be considered as provisional. Considerable experimental data from other sources support the view that the dimeric class I synthetases (TrpRS and TyrRS) must transmit information from the active site on one monomer across the dimer interface (Bedouelle & Winter, 1986; Carter et al., 1986; Labouze & Bedouelle, 1989; Bedouelle, 1990). Such intramolecular signaling is necessary to coordinate the movements of the anticodon-binding region believed to involve the SD. Evidence obtained for the closely related *Bacillus subtilis* TrpRS by fluorescence measurements (Hogue et al., 1996) and by chemical modification (Xue et al., 1997) have previously been interpreted as indicating such communication. It is remarkable that substantial changes in conformational angles between the two TrpRS conformations are exclusively localized to the two belts and the two regions previously implicated in tRNA[Trp] binding. However, additional structural data will be required to resolve this question.

Methods

Small angle X-ray scattering

The design matrix of this experiment was similar to that described in Carter et al. (1994), except that experiments were carried out at different TrpRS concentrations, but at the same temperature ($\sim$21°C). Thus, solution scattering experiments involved joint, full-factorial variation of pH and the enzyme, tryptophan, and ATP concentrations. X-ray scattering patterns were recorded on the Small-Angle X-ray Scattering (SAXS) instrument D24 using the emission from a bending magnet on the storage ring DCI at LURE (Orsay, France) and previously described methods (Fetler et al., 1997). The instrument (Depautex et al., 1987), the acquisition program (Boulin et al., 1986), and the evacuated measuring cell (Dubuisson et al., 1997) have been described. Radii of gyration for multiple replicates of the 16 different experimental conditions were estimated from selected, linear portions of Guinier plots (Guinier, 1963).
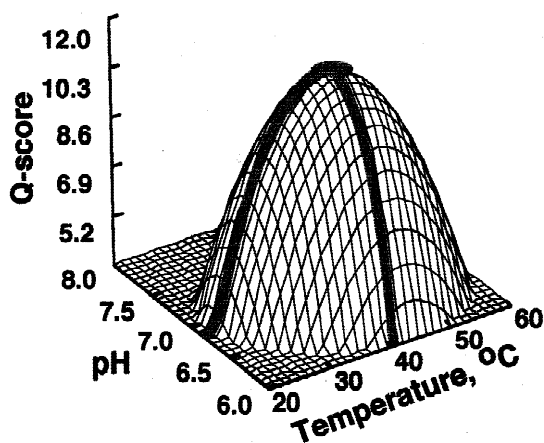
Fig. 9. Response surface for ligand-free TrpRS crystals. Four variables, including pH, temperature, [protein], and [PEG400] were examined using a 20-experiment Hardin-Sloane design (Carter & Yin, 1994). Analysis of scores based on a scheme of relative crystal quality (Carter & Carter, 1979) yielded a model with optima for all four variables ($R^2 = 0.90$; F-ratio probability 0.002). The pH temperature level surface: $Q = -728 + 3.36 * T + 198.4 * pH - 0.22 * T * pH - 0.02 * T^2 - 14.0 * pH^2$ is plotted at optimum values for the protein (5.6 mg/mL) and PEG400 (0.6%) concentrations.

Fig. 10. Schematic representation of the maximum-entropy omit-map algorithm used for model-independent phase refinement.

Crystallization

The thermostable TrpRS was crystallized by microdialysis. Systematic response-surface analysis of the crystal growth conditions (G. Li, unpubl. obs.) revealed an optimum growth in ~2.0 M K_2HPO_4 at pH = 6.8. and at 315 K (Fig. 9). This temperature optimum is consistent with the thermophilic origin of the enzyme. Unit cell dimensions and 32 noncrystallographic symmetry in both asymmetric units are very similar to those previously observed for monoclinic (P21) crystals of crystals grown in the presence of tryptophan (Carter et al., 1990). Both triclinic and monoclinic crystal forms grew under identical conditions.

Complete data sets to about 3.2 A for P1 and 2.9 A for C2 were collected from a single crystal for each crystal from. Calculation of self-rotation function revealed the 32 local symmetry of the trimer-dimer; three noncrystallographic twofold axes were found approximately 120° apart, perpendicular to the noncrystallographic threefold axis, which lies nearly along a^* and is perpendicular to the crystallographic b-axis in C2.

Structure solution

Previous experience had suggested that we could not make heavy-atom derivatives without loss of isomorphism (Doublié et al., 1994). By the same token, it is well known (Hodel et al., 1992; Read, 1997) that biases from an initial model used in molecular replacement propagate into the final model unless strong measures are taken to reverse them. We therefore solved this structure by combining molecular replacement and a phase/map refinement method based on Maximum Entropy Solvent Flattening (Xiang et al., 1993) together with noncrystallographic averaging and phase permutation (Doublié et al., 1995) (Fig. 10).

Initial phases were obtained by molecular replacement using a 2.8 Å structure of ligand-free TrpRS from a tetragonal crystal from which ligand had diffused away (Yin, 1995). That structure had
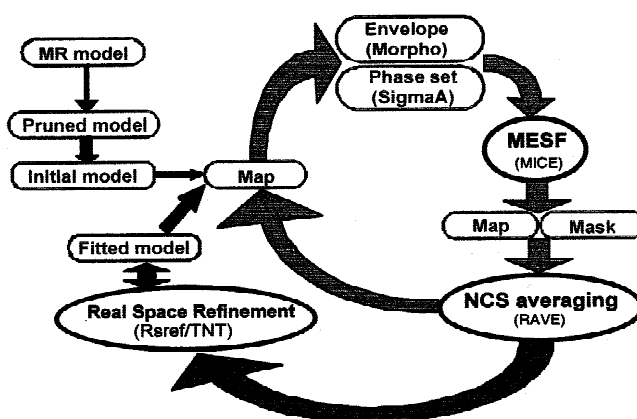
undergone an outward movement of the helical domain, suggesting that its structure might be closer to the ligand-free structure in C2 crystals. (This assumption proved to be false. Despite the fact that the domain movement resembled that which we observed in the present unliganded TrpRs structure, crystal packing in the tetragonal structure distorted the structures of both domains sufficiently that the structure used was actually a worse molecular replacement model than was the previously solved structure of the TAM complex.) Rotation and translation searches with AMORE (Navaza, 1997) readily placed this model without ambiguity for all resolution ranges tested, showing that each asymmetric unit contains either one (C2) or two (P1) units of three enzyme dimers related by 3_1 screw symmetry. The current structure was solved in crystal form C2 with six monomers per asymmetric unit because the X-ray intensities extended to higher resolution. The six monomers in the C2 crystal asymmetric unit associate to form three dimers (A–D, B–E, C–F) related by an approximate 3_1 screw axis with respective rotations of 117.3°, 123.5°, and 119.2° and translations of 33.0, 23.6, and 28.7 Å.

Both crystal forms have calculated V_m values of 2.71 $A^3 Da^{-1}$ and are closely related to space group $P3_121$, previously observed at 18 Å resolution in $P2_1$ crystals and, mistakenly, thought to belong to space group P321 (Carter et al., 1990).

The monomer was divided into two parts for rigid body refinement: the Rossmann fold and C-terminal helix (residues 1–175; 295–326), the four-helix bundle (residues 176–293). Rigid-body domain refinements improved the map quality sufficiently to identify polypeptide chain for most of the Rossmann fold and the helical domains (Fig. 12A), but we were still unable to place the remaining ~20% of the molecule, located mainly between these two domains. Residue-by-residue real-space correlation coefficients of this model with the corresponding $2F_o - F_c$ map (Fig. 11A) formed a normal distribution centered on 0.6, which accounted for 80% of the structure, and a tail representing serious, systematic coordinate errors from the molecular replacement model in the remaining structure (Fig. 11B). The worst phase biases from the initial model were eliminated by removing residues whose correlation coefficients were below the normal distribution, namely those less than 0.35. This truncated model was used to initiate map improvement.

Map/phase improvement proceeded iteratively, with joint application of noncrystallographic symmetry, solvent flattening, and
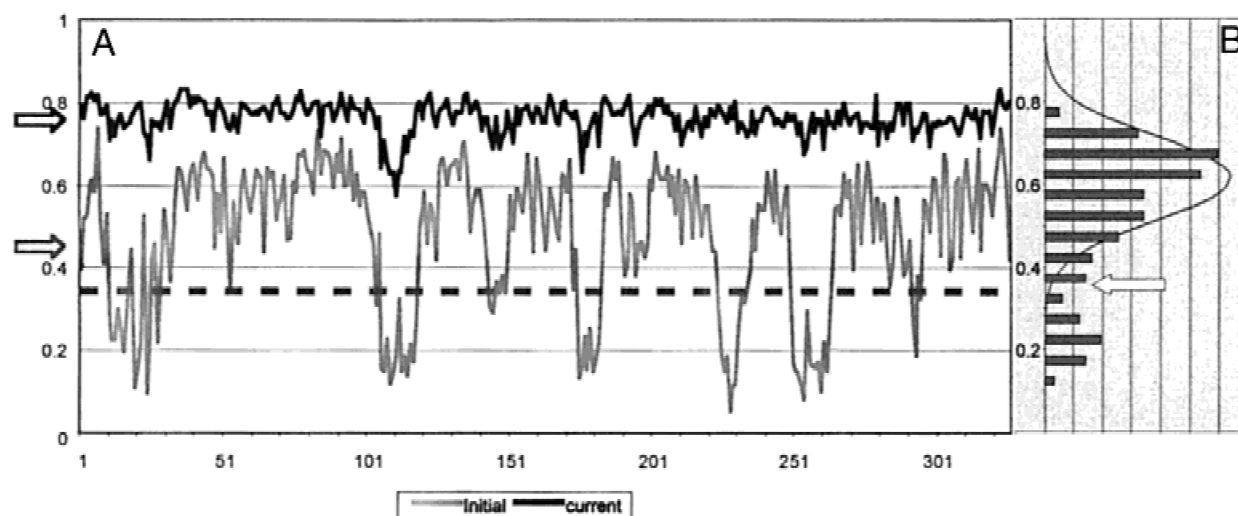
Fig. 11. **A:** Real-space correlation coefficients, calculated by function rs_fit in program O. (Lower trace) Correlation between initial molecular replacement model and its sigmaA-weighted $\{2|F_{obs}| - |F_{calc}|, \phi_{calc}\}$ electron density map. Dashed line indicates the cutoff, determined from the histogram in **B** for pruning the molecular replacement model. (Upper trace) Correlation between final model and the final, sigmaA-weighted $\{2|F_{obs}| - |F_{calc}|, \phi_{calc}\}$ map. Mean overall correlation coefficients are indicated with arrows on left-hand side. **B:** Frequency distribution of correlation coefficient between initial model and density. Arrow denotes the threshhold below which atoms lie outside a normal distribution, and hence, indicate systematic coordinate errors resulting from the molecular replacement phases.

maximum entropy constraints. Because a full implementation of this Bayesian paradigm is still under development (Bricogne, 1998), we approximated it as shown in Figure 10. A "metacycle" of map improvement consisted of computing using MICE (Xiang et al., 1993) and averaging (Kleywegt & Jones, 1996) "maximum entropy omit maps," followed by adjustment of the model using

automated (Chapman, 1995) and manual rebuilding. By analogy with the use of "omit maps" in real space (Bhat, 1988), we eliminated two-thirds of the phased reflections from the list of constraints for each cycle of entropy maximization, retaining only those reflections with highest Sim weight, rather than omitting parts of the model.

Table 4. *Phase permutation experiments*

Variable	Coefficient	Standard error	Student t	P(2 tail)	Phi	R^2	F-ratio	p
Perm 1								
$N = 40/4{,}096$						0.964	76.9	0.99E−15
I(−13,−1,9)	−44.4	3.058	−14.5	0.80E−14	270			
R(−2,−4,6)	38.5	2.956	13.0	0.12E−12				
I(−2,−4,6)	−12.8	2.889	−4.4	0.13E−03	342			
R(1,5,3)	19.0	2.698	7.1	0.97E−07				
I(1,5,3)	−32.7	2.738	−11.9	0.10E−11	300			
R(−4,−6,4)	−10.1	2.853	−3.6	0.001				
I(−4,−6,4)	38.7	2.771	14.0	0.21E−13	105			
R(0,6,2)	−8.5	2.777	−3.0	0.005	180			
R(0,6,0)	−17.5	2.999	−5.9	0.24E−05				
I(0,6,0)	5.2	2.757	1.9	0.070	164			
Perm 2								
$N = 32/2{,}048$						0.968	103.9	0.99E−15
R(−10,−4,4)	−7.0	1.706	−4.1	0.38E−03				
I(−10,−4,4)	−36.7	1.722	−21.3	0.10E−14	259			
R(−9,−3,9)	22.8	1.615	14.1	0.41E−12				
I(−9,−3,9)	5.3	1.575	3.4	0.003	13			
R(−7,−5,3)	6.5	1.707	3.8	0.92E−03				
I(−7,−5,3)	13.8	1.689	8.2	0.22E−07	65			
S(−2,0,8)	−8.7	1.661	−5.2	0.22E−04	180			

The map/phase improvement convergenced initially with over-all correlation between map and model of around 0.6. Then we evaluated the resulting set of structure factors using a cosine law approximation to the transform of the residual error in the map $|U_{renorm}| = (|U_{obs}|^2 + |U^{ME}|^2 - 2\,|U_{obs}||U^{ME}|\,W_{tsim})^{1/2}$. We twice permuted phases (Table 4) for the 16 reflections with the largest $|U_{renorm}|$. [We also identified several (three) reflections whose structure factors had very large $|U_{renorm}|$ because $|U_{obs}| \ll |U^{ME}|$. These low-resolution structure factors represented errors in measurement, and were deleted from the data set.] The procedure and evaluation have been described elsewhere (Doublié et al., 1994). Predicted values of the log-likelihood gain (LLG) from the permutation were in very good agreement with actual calculations after each phase correction. Reflections missing $|U_{obs}|$ were estimated as $|U^{ME}|$. Direct phasing of reflections by permutation experiments increased the maximum LLG, significantly improved the interpretability 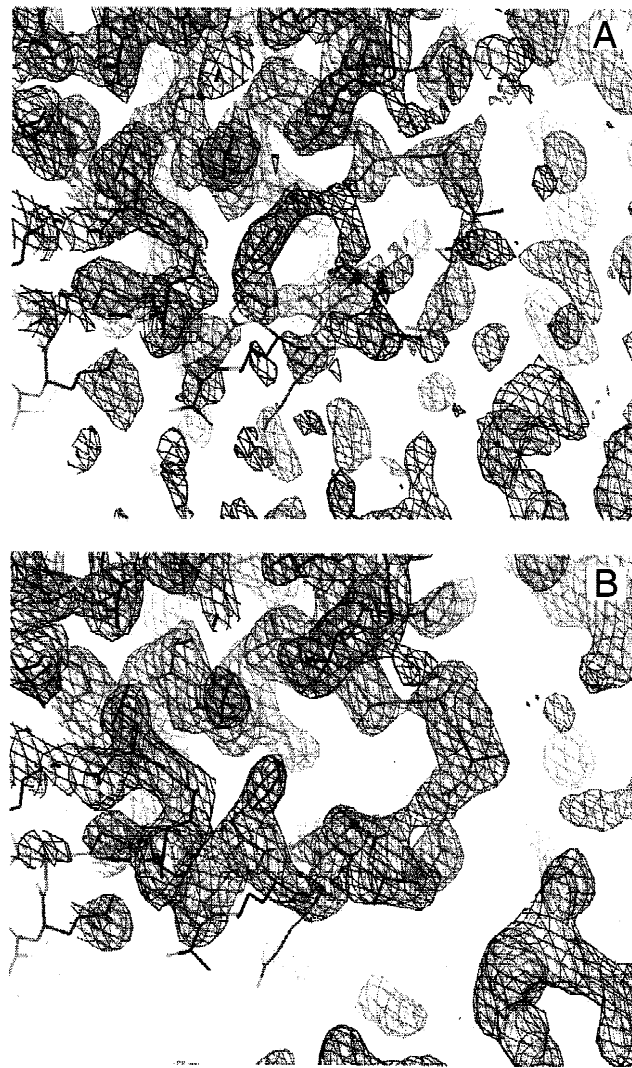of the electron density map as shown in Figure 12B, and increased the correlation between the model and the map from 0.47 to 0.61.

This approach to phase determination allowed us to refine phases essentially to convergence before refining model coordinates. We rebuilt the model into improved maps only after the map improvement converged for all parameters. Automated model building using Rsref/TNT (Chapman, 1995), aided by partial manual rebuilding, produced a high quality structure. When the entire process of local model building and map improvement converged, the model had a mean real-space correlation of 0.74 and an R_{factor}/R_{free} of 0.29, coordinate refinement with CNS (Brünger, 1988; Rice & Brünger, 1994), using torsional dynamics with maximum likelihood targets (Pannu & Read, 1996) and noncrystallographic symmetry constraints for 18 domains resulted in a model with $R_{factor} = 0.24$ and $R_{free} = 0.26$ (Protein Data Bank access code 1D2R). Further refinement increased R_{free} and was not pursued.

Supplementary material in Electronic Appendix

Eight kinemages animate comparisons of the crystal structures and are arranged in the order in which they are discussed in the text:

1. Overview of the TrpR Rossmann dinucleotide binding fold.

2. Structural polymorphism in the six independent TrpRS monomers.

3. Conformational differences between ligand-free TrpRS and the TAM complex.

4–5. Flexion of the C-terminal helices 265–293 and 294–325 between ligand-free TrpRS and the TAM complex.

6. Active-site changes between ligand-free TrpRS and the TAM complex.

7. Nonpolar repacking associated with the conformational differences.

8. Comparison of native, dimeric ligand-free, and TAM complexed TrpRS.

Acknowledgments

Fig. 12. Model-independent electron density map improvement. **A:** Initial molecular replacement sigmaA-weighted $\{2|F_{obs}| - |F_{calc}|, \phi_{calc}\}$ map and final coordinates. **B:** Map after maximum-entropy omit-map phase refinement (Fig. 12), but before automated coordinate refinement (RSREF/TNT, CNS). In both maps, contours are drawn at 1.0σ.

References

Baldwin J, Chothia C. 1979. Hemoglobin: The structural change related to ligand-binding and its allosteric mechanism. *J Mol Biol 129*:179–220.

Bedouelle H. 1990. Recognition of tRNA^{tyr} by tyrosyl-tRNA synthetase. *Biochimie 72*:589–598.

Bedouelle H, Winter G. 1986. A model of synthetase/transfer RNA interaction as deduced by protein engineering. *Nature 230*:371–373.

Bhat TN. 1988. Calculation of an OMIT MAP. *J Appl Crystallogr 21*:279–281.

Boulin C, Kempf R, Koch MHJ, McLaughlin SM. 1986. Data appraisal, evaluation and display for synchrotron radiation experiments: Hardware and software. *Nucl Instrum Methods A249*:399–407.

Brick P, Bhat TN, Blow DM. 1988. Structure of tyrosyl-tRNA synthetase refined at 2.3 Å resolution: Interaction of the enzyme with the tyrosyl adenylate intermediate. *J Mol Biol 208*:83–98.

Bricogne G. 1998. Bayesian statistical viewpoint on structure determination: Basic concepts and examples. *Methods Enzymol 276*:361–423.

Brünger AJ. 1988. Crystallographic refinement by simulated annealing. Application to a 2.8 Å resolution structure of aspartate aminotransferase. *J Mol Biol 203*:803–816.

Burbaum JJ, Schimmel P. 1992. Amino acid binding by the class I aminoacyl-tRNA synthetases: Role for a conserved proline in the signature sequence. *Protein Sci 1*:575–581.

Burbaum JJ, Starzyk RM, Schimmel P. 1990. Understanding structural relationships in proteins of unsolved three-dimensional structure. *Proteins Struct Funct Genet 7*:99–111.

Carter CW Jr. 1993. Cognition, mechanism, and evolutionary relationships in aminoacyl-tRNA synthetases. *Annu Rev Biochem 62*:715–748.

Carter CW Jr, Carter CW. 1979. Protein crystallization using incomplete factorial experiments. *J Biol Chem 254*:12219–12223.

Carter CW Jr, Crumley KV, Coleman DE, Hage F, Bricogne G. 1990. Direct phase determination for the molecular envelope of tryptophanyl-tRNA synthetase from *Bacillus stearothermophilus. Acta Crystallogr A46*:57–68.

Carter CW Jr, Doublié S, Coleman DE. 1994. Quantitative analysis of crystal growth: Tryptophanyl-tRNA synthetase polymorphism and its relationship to catalysis. *J Mol Biol 238*:346–365.

Carter CW Jr, Ilyin VA, Huang X, Yin Y, Hu M, Longo A, Retailleau P. 1999. TRPRS: Three-state behavior, induced-fit, intramolecular signaling, and free-energy transduction. *Acta Crystallog A55 Suppl*. Forthcoming.

Carter CW Jr, Yin Y. 1994. Quantitative analysis in the characterization and optimization of protein crystal growth. *Acta Crystallogr D50*:572–590.

Carter P, Bedouelle H, Winter G. 1986. Construction of heterodimer tyrosyl-tRNA synthetase shows tRNA^Tyr interacts with both subunits. *Proc Natl Acad Sci USA 83*:1189–1192.

Chapman MS. 1995. Restrained real-space macromolecular atomic refinement using a new resolution-dependent electron density function. *Acta Crystallogr A51*:69–80.

Depautex C, Desvignes C, Leboucher P, Lemonnier M, Dagneaux D, Benoit J-P, Vachette P. 1987. The small angle scattering instrument D24. *LURE Annual Report 1985–1987*:2075.

Doublié S, Bricogne G, Gilmore CJ, Carter CW Jr. 1995. Tryptophanyl-tRNA synthetase crystal structure reveals an unexpected homology to Tyrosyl-tRNA synthetase. *Structure 3*:17–31.

Doublié S, Xiang S, Gilmore CJ, Bricogne G, Carter CW Jr. 1994. Overcoming nonisomorphism by phase permutation and likelihood scoring: Solution of the TrpRS crystal structure. *Acta Crystallogr A50*:164–182.

Dubuisson J-M, Decamps T, Vachette P. 1997. Improved signal-to-background ratio in small-angle X-ray scattering experiments with synchrotron radiation using an evacuated cell for solutions. *J Appl Crystallogr 30*:781–786.

Fersht A. 1988. Dissection of the structure and activity of an enzyme. In Kaiser ET, ed. *Design of enzymes and enzyme models*, vol. XXXI. Houston, Texas: Robert A. Welch Foundation. pp 159–182.

Fersht AR. 1987. Dissection of the structure and activity of the tyrosyl-tRNA synthetase by site-directed mutagenesis. *Biochemistry 26*:8031–8037.

Fersht AR, Knill-Jones JW, Bedouelle H, Winter G. 1988. Reconstruction by site-directed mutagenesis of the transition state for the activation of tyrosine by the tyrosyl-tRNA synthetase: A mobile loop envelopes the transition state in an induced-fit mechanism. *Biochemistry 27*:1581–1587.

Fetler L, Tauc P, Vachette P. 1997. Carbamoyl phosphate modifies the T quaternary structure of aspartate transcarbamylase, thereby facilitating the structural transition associated with cooperativity. *J Appl Crystallogr 30*:781–786.

Guinier A. 1963. *X-ray diffraction in crystals, imperfect crystals, and amorphous bodies*. New York: W.H. Freeman and Company.

Hodel A, Kim S-H, Brünger AT. 1992. Model bias in macromolecular crystal structures. *Acta Crystallogr A48*:851–855.

Hogue CWV, Doublié S, Xue H, Wong J, Carter CW Jr, Szabo AG. 1996. A concerted, tryptophanyl-adenylate dependent conformational change in *B. subtilis* tryptophanyl-tRNA synthetase revealed by the fluorescence of tryptophan 92. *J Mol Biol 260*:446–466.

Hountondji C, Dessen P, Blanquet S. 1986. Sequence similarities among the family of aminoacyl-tRNA synthetases. *Biochimie 68*:1071–1078.

Ilyin V. 1994. Nonpolar regions in fungal microbial ribonucleases. *Protein Eng 7*:1189–1195.

Jahn M, Rogers MJ, Söll D. 1991. Anticodon and acceptor stem nucleotides in tRNA^Gln are major recognition elements for *E. coli* glutaminyl-tRNA synthetase. *Nature 352*:258–260.

Kleywegt GJ, Jones TA. 1996. Use of non-crystallographic symmetry in protein structure refinement. *Acta Crystallogr D52*:842–857.

Labouze E, Bedouelle H. 1989. Structural and kinetic bases for the recognition of tRNA^Tyr by tyrosyl-tRNA synthetase. *J Mol Biol 205*:729–735.

Navaza J. 1997. AMoRe: An automated molecular replacement package. *Methods Enzymol 276*:581–594.

Pannu NS, Read RJ. 1996. Improved structure refinement through maximum likelihood. *Acta Crystallogr A52*:659–668.

Read RJ. 1997. Model phases: Probabilities and bias. *Methods Enzymol 277*. Forthcoming.

Rice L, Brünger A. 1994. Torsion angle dynamics: Reduced variable conformational sampling enhances crystallographic refinement. *Proteins Struct Funct Genet 19*:277–290.

Rould M, Perona JJ, Steitz T. 1989. High resolution crystal structure of *E. coli* glutaminyl-tRNA synthetase complexed with its cognate tRNA. *Biophys J 55*:49a.

Rould MA, Steitz TA. 1992. Structure of the glutaminyl-tRNA synthetase–tRNA^Gln complex. In Eckstein F, Lilley DMJ, eds. *Nucleic acids and molecular biology*, vol. 6. Berlin: Springer Verlag. pp 225–246.

Schulman LH, Pelka H. 1988. Anticodon switching changes the identity of methionine and valine transfer RNAs. *Science 242*:765–768.

Schulman LH, Pelka H. 1989. The anticodon contains a major element of the identity of arginine transfer RNAs. *Science 246*:1595–1597.

Senger B, Despons L, Walter P, Fasiolo F. 1992. The anticodon loop and the discriminatory base determine the methionine acceptance of yeast tRNA^Met. *Proc Natl Acad Sci USA 89*:10768–10771.

Ward WHJ, Fersht AR. 1988a. Asymmetry of tyrosyl-tRNA synthetase in solution. *Biochemistry 27*:1041–1049.

Ward WHJ, Fersht AR. 1988b. Tyrosyl-tRNA synthetase acts as an asymmetric dimer in charging tRNA. A rationale for half-of-the-sites activity. *Biochemistry 27*:5525–5530.

Webster T, Tsai H, Kula M, Mackie GA, Schimmel P. 1984. Specific sequence holmology and three-dimensional structure of an aminoacyl transfer RNA synthetase. *Science 226*:1315–1317.

Xiang S, Carter CW Jr, Bricogne G, Gilmore CJ. 1993. Entropy maximization constrained by solvent flatness: A new method for macromolecular phase extension and map improvement. *Acta Crystallogr D49*:193–212.

Xue H, Xue Y, Doublié S, Carter CW Jr. 1997. Chemical modifications of *Bacillus subtilis* tryptophanyl-tRNA synthetase. *Biochem Cell Biol 75*:709–715.

Yesland KD, Johnson JD. 1993. Anticodon bases C34 and C35 are major, positive, identity elements in *Saccharomyces cerevisiae* tRNA(Trp). *Nucleic Acids Res 21*:5079–5084.

Yin Y. 1995. Crystallographic study of *Bacillus stearothermophilus* tryptophanyl-tRNA synthetase in the catalytic reaction [PhD thesis]. University of North Carolina at Chapel Hill.